Special Section on PG Gems

Illumination Browser: An intuitive representation for radiance map databases

Andrew Chalmers [a,*], Todd Zickler [b], Taehyun Rhee [a]

[a] *Computational Media Innovation Centre, Wellington, New Zealand*
[b] *Harvard University, Cambridge, MA, United States of America*

ARTICLE INFO

ABSTRACT

Radiance maps (RM) are used for capturing the lighting properties of real-world environments. Databases of RMs are useful for various rendering applications such as look development, live action composition, mixed reality, and machine learning. Such databases are not useful if they cannot be organized in a meaningful way. To address this, we introduce the illumination space, a feature space that arranges RM databases based on illumination properties. Our method is motivated by how the RM illuminates the scene as opposed to describing the textural content of the RM. We avoid manual labeling by automatically extracting features from an RM that provides a concise and semantically meaningful representation of its typical lighting effects. We also introduce 'Illumination Browser', a user interface (UI) that visualizes the illumination space alongside a real-time preview renderer to enable intuitive browsing for artists. This is made possible with the following contributions: a method to automatically extract a small set of dominant and ambient lighting properties from RMs, a low-dimensional (5D) *light feature* vector summarizing these properties to form the illumination space, and a UI that effectively utilizes the illumination space.

1. Introduction

Radiance maps (RMs) are high dynamic range (HDR) 360° images that are suitable for storing real-world lighting. Databases of RMs are now readily available in post-production studios and online services, providing a large amount of high fidelity illumination data. Current machine learning methods use RM databases for unsupervised learning tasks [1–3]. However, an unlabeled database of RMs is not useful in many other lighting applications that require searching or browsing the database (e.g., Look Development, live action composition, mixed reality rendering, and supervised learning). Furthermore, the labels should be concise to avoid sparsity introduced by high-dimensional data (i.e. the curse of dimensionality). An intuitive, low-dimensional representation that describes lighting, not texture, is required for many of these applications. This representation also requires an intuitive interface to enable artists to utilize the feature space. Describing and visualizing an RM in concise form is challenging since each RM contains a variety of complex lighting properties including shading, tone, shadows, and glossy highlights.

Current models either do not provide enough semantically meaningful parameters (e.g., Hosek–Wilkie [4] does not cover overcast skies or indoor lighting), or provide too many unintuitive parameters (e.g., spherical harmonics [5]). Our prior work [6] utilized spherical Gaussians (SG) [7,8] and diffuse shading to develop an 'illumination space', which we extend into 'Illumination Browser' to visualize RM databases with an intuitive interface for browsing and searching applications. The browser contains a real-time preview renderer to visualize the mirror/glossy/diffuse effect of a selected RM. The low dimensional representation aims to capture properties that are observable in the rendered scene rather than the textural content of the RM image itself. To obtain a low-dimensional representation, we utilize a dominant light model (DLM) which uses SGs to describe the most visually salient lighting effects as observed in the rendered scene. Diffuse shading is then used to capture semantically meaningful, low-dimensional tonal properties.

To develop a low-dimensional representation, we follow an empirical approach of making careful design decisions and observing their effects in large RM databases. Numerous iterations of this design process lead us to five intuitive lighting properties of RMs, split into two categories, *dominant* and *ambient* lighting: the (1) **size**, (2) **elevation angle**, and (3) **azimuth angle** of the RM's most dominant area light sources, as well as the diffuse (4) **hue** and (5) **saturation** of the RM. The dominant lighting property set (1, 2, 3) can occur multiple times for a given RM (one set for
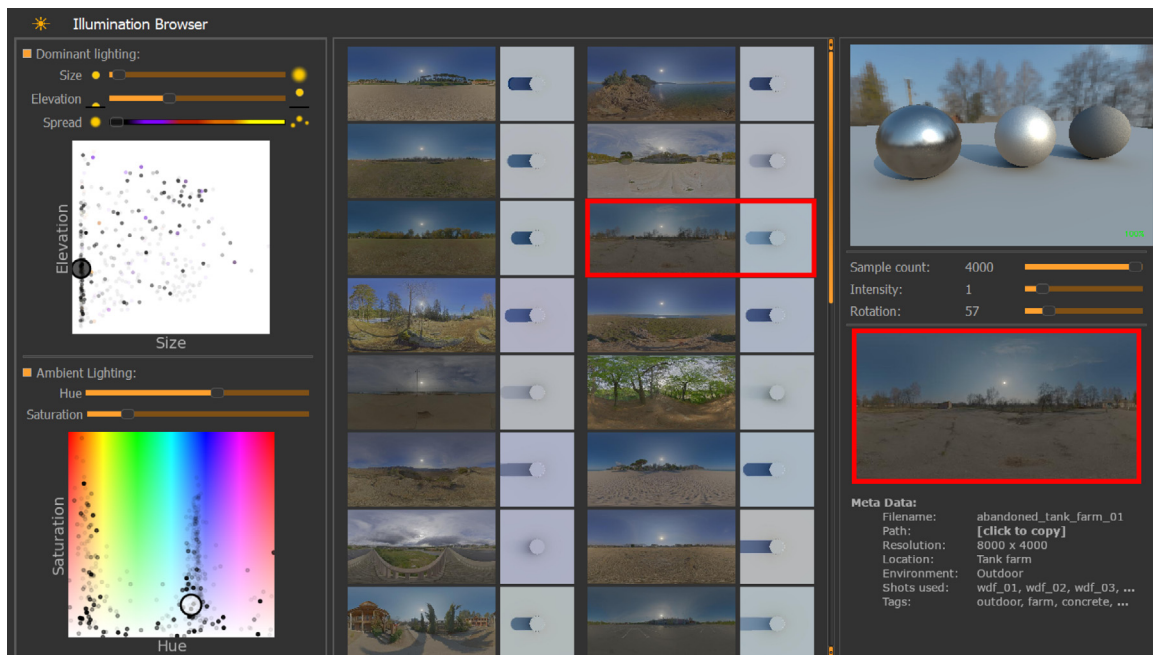
Fig. 1. The 'Illumination Browser' interface. The left panel contains the 'illumination space', a low dimensional feature space visualized as scatterplot graphs (top: dominant lighting, bottom: ambient lighting). Each point in the scatterplot represents a radiance map. The user places the cursor (large circles) inside the scatterplots to query the database. The center panel shows the retrieved radiance maps (alongside a preview rendering of a top-down cylinder scene illustrating the diffuse tone and shadow profile) closest to the input query. The user can select a radiance map in the center panel (e.g., the red square outline). The right panel uses the selected radiance map in a real-time path tracer of 3 spheres with different materials and a shadow catching plane.

each bright light in the RM). To create a low-dimensional feature space, these properties are converted into a strictly 5D feature vector. This defines the *'illumination space'* - a semantically meaningful, low-dimensional feature space. This feature space is embedded in our proposed *'Illumination Browser'* interface (see Fig. 1) to enable browsing RM databases. Our contributions are summarized as follows:

- We define and extract a small set of dominant and ambient lighting properties from RMs using the DLM.
- From the extracted lighting properties, we introduce a 5D *light feature* vector that encodes RMs in a low-dimensional, semantically meaningful feature space — the *'illumination space'*.
- *'Illumination Browser'* is presented, an interactive visualization for browsing an RM database. Alongside browsing, we also demonstrate searching the RM database by using an RM to obtain other similar RMs.

2. Related work

2.1. Dimensionality reduction

Dimensionality reduction is a long-standing research area which aims to reduce high-dimensional data into a low-dimensional space. Principal component analysis (PCA) and multidimensional scaling (MDS) [9] is often used for this task, and has been successfully used in semantic image browsing applications [10,11]. More recently, t-distributed stochastic neighbor embedding (t-SNE) [12] has been used specifically for visualizing high dimensional data, with recent work applying variations of t-SNE to browse textures [13]. Since we are interested in the rendering effect of radiance maps, applying such dimensionality reduction techniques directly to radiance maps does not capture the rendering effect well (which we demonstrate in the supplementary file). We instead use feature extraction that directly obtains the lighting features users are interested in.

2.2. Textural features for sky images

Manual labels applied to images (or parts of images) can guide browsing and searching in many applications [14–16]. Labels extracted from the metadata attached to images at capture time can also be used. However, these sorts of labels have limited expressibility and are not always available, so features computed from image content—such as GIST [17], geometric context [18], and spatial pyramids [19]—are often used instead. When they are applied to an RM, we refer to these as "textural features" because they are computed from the contrast patterns of the RM itself, instead of the lighting patterns that the RM induces in a rendered scene. Tao et al. [20] use textural features and supervised learning techniques to develop an interactive search system for finding sky photographs. Ono et al. [21] extract four textural features to characterize the images in a database, with ongoing improvements for sky searching and generation [16,22]. Similarly, Chalmers et al. [23] use textural features to enable artists to find backdrops with various amounts and types of clouds. A substantial limitation of textural features is that they often do not adequately encode an RM's lighting effects. This is what we aim to address in this paper.

2.3. Perceptual embeddings

There is a long history of creating low-dimensional and perceptually meaningful embeddings of materials for digital design and editing tasks. The 1976 CIELAB representation of color is an early example. More recent examples include perceptual embeddings of reflectance [24–26] and translucency [27,28]. We follow this same general strategy, albeit for studying illumination – and RMs in particular – instead of materials. Previous encodings for RMs have considered dimensionality reduction without perceptual uniformity [29], or have relied on the manual attachment of tags [30], such as sun position and color, which is difficult to extend to large databases and the many possible attributes of appearance.

2.4. Light estimation

A distinct but related task is that of estimating (from within some continuous, parameterized space of RMs) an RM that matches a given photograph. Examples include estimating an analytical sky model [2,31,32], spherical Gaussian-like parameters [33], spherical harmonics [34], or a higher-dimensional, pixel-based RM representation from a photograph [1,35–38]. A survey on this topic is provided by [39]. Light estimation allows for creating a new RM instance that matches a specific target photograph, but it does not provide artists with the ability to browse an RM database to find artistically-pleasing rendering results, nor does it allow the artist to make corrections if the estimated RM instance induces undesirable rendering effects. However, such methods work in harmony with our illumination space since they provide a good starting point for artists to browse from, or to use the RM estimate as a search query to return a similar but high quality real-world RM.

2.5. Sampling and compression for RMs

Frequency space representations have been used to compress RMs down to as few as nine [5,40] or hundreds [41] coefficients with varying degrees of fidelity. Our 5D light feature vector instead describes both high and low frequency lighting in a semantically meaningful way with fewer parameters. Sampling algorithms sample areas of interest in the RM [42–45], however, these sampling methods aim to oversample the area of interest rather than sample the light source once with a low-dimensional descriptor.

2.6. Radiance map datasets

Previous work have produced RM datasets containing indoor [1], outdoor [46], or a combination [35,47]. RM datasets are also available online [48–54]. In our experiments, we use the HDRI-Haven [48], Dutch Skies [51] and the Lavel Indoor [1] datasets.

3. Dominant light definition

Before introducing the 5D light feature vector, we first define how we obtain dominant lighting properties, which we then use to encode into the dominant light features. A dominant light in an RM is a local region of the lighting sphere $\Omega \subset \mathbb{S}^2$ with the property that the region has a substantial impact on high-frequency lighting effects in a scene, including highlights and cast shadows. An RM may have multiple dominant lights, and we use Ω_j to denote the jth dominant light. We assume light Ω_j is given through a light detection scheme; we use statistics-based thresholding defined by Rhee et al. [55]. The remainder of this section introduces the dominant light model (DLM) for summarizing the lighting effects of each Ω_j, and the procedure of fitting a DLM to each Ω_j (resulting in a DLM for each dominant light source in an RM). Section 4.1 shows how the fitted parameters of each DLM are summarized into a dominant light feature vector used in the illumination space.

3.1. Dominant Light Model (DLM)

To extract the elevation and size of a dominant light Ω_j, the first step is to fit a parametric model to each Ω_j. While we are only interested in a lower dimensional representation that Spherical Gaussians (SG) [7] provide, we use Anisotropic Spherical Gaussians (ASG) [8] since they often provide a better fit. We then

reduce the ASG back into a SG. The ASG is defined as a function given a unit direction $\mathbf{v}$ and light intensity a:

$$G(\mathbf{v}, a; [\mathbf{x}, \mathbf{y}, \mathbf{z}], [\sigma_x, \sigma_y]) = a \cdot \max(\mathbf{v} \cdot \mathbf{z}, 0) \cdot e^{-\sigma_x(\mathbf{v} \cdot \mathbf{x})^2 - \sigma_y(\mathbf{v} \cdot \mathbf{y})^2} \quad (1)$$

The vectors $\mathbf{x}, \mathbf{y}, \mathbf{z} \in \mathbb{S}^2$ are the tangent, bi-tangent, and lobe direction axes respectively, forming an orthogonal basis of $\mathbf{R}^3$, with z being the 'direction' of the dominant light relative to objects in a rendered scene , and the other two axis defining the anisotropic orientation. The parameters σ_x and σ_y define the size of the Gaussian for the x and y axes respectively (where $\sigma_x, \sigma_y > 0$), and a is the light intensity. The ASG is reduced into a SG by averaging σ_x and σ_y.

3.2. DLM fitting

The process of fitting $G(\mathbf{v}, a; \mathbf{p})$ (where $\mathbf{p}$ are the parameters of a DLM) to a dominant light source provides an automatic parameterization of real-world lighting. This optimization minimizes the difference between the gray-scale intensities in the RM and the DLM's approximation of it. From the fitted $G(\mathbf{v}, a; \mathbf{p})$, we extract the light features that describe the real-world illumination properties. To fit $G(\mathbf{v}, a; \mathbf{p})$ to a gray-scale RM, we first initialize, then optimize.

The input parameters $\mathbf{v}$ and a are given from the direction of the local maxima and the gray-scale intensity of the pixel in the RM from the corresponding direction. The remaining parameters $\mathbf{p}$ from Eq. (1) are given an initial approximation (as well as upper and lower bounds) and are optimized. σ_x and σ_y are initialized to be radially symmetric with a solid angle of $0.5334°$ (the solid angle of the sun as observed from Earth), and a lower and upper limit of $0.5334°$ and $90°$ respectively. Experimentally we found that the optimization ran faster and more robustly when an initialization and bounds were given. We use the sun as a reference as this is a known object that appears regularly in the dataset. An upper-bound of $90°$ is used as it is unusual to find a light source larger than this size. The anisotropic orientation of the DLM is initialized to 0 with a lower and upper limit of $0°$ and $360°$ respectively. Given the initialization parameters and boundary conditions, the parameters $\mathbf{p}$ are optimized using the dog-leg trust-region algorithm [56] with the objective function

$$f(l, g) = \frac{1}{N} \sum_i w_i(l_i - g_i) \quad (2)$$

where i is an index into each pixel, l is the RM and g is the current approximation of l generated by combining all DLMs (we combine them taking the maximum intensity value across the DLMs at each location i). We use w as a weight for each pixel based on its corresponding solid angle to account for the distortion at the poles of an equirectangular image.

3.3. DLM shadow transform

The ASG fits the intensity values directly from the RM. However, it is useful to not only describe the size of the light, but also the light's shadowing effect. In 'Illumination Browser', the canonical occluder "shadow image" (a top-down orthographic view of a cylinder on a plane, resembling a sun dial. See Fig. 1-center panel, and the supplementary materials) is shown to the user while they browse. However, a linear change in the light's size will not correspond to a linear change in the shadow's softness (which is what the user is looking at while browsing in our system). A light's size, as well as the direction of the light relative to an occluder affects the shadow's softness. In the case of the "shadow image", the shadows from lights with lower elevations spread across a wider area, creating a softer shadow. With this observation, and using a canonical occluder, we can encode the
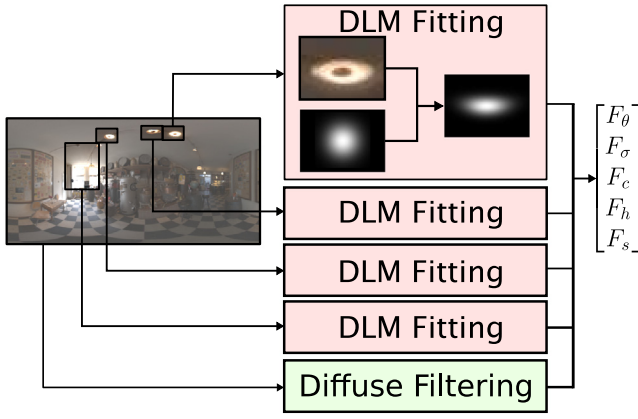
Fig. 2. Feature extraction process. Given an input RM, each dominant light is fit with the DLM (red boxes). The RM itself is also diffusely filtered (green box). Then the elevation θ and size σ properties from each DLM are aggregated into three dominant lighting features F_θ, F_σ, and F_c. The hue and saturation features F_h and F_s are computed from the diffusely filtered RM.

RM's shadowing properties intuitively and consistently across the database. To obtain this effect, we perform a 1D transformation of the SG into a shadow profile:

$$\sigma' = \frac{1}{\tan(\theta - \frac{\sigma}{2})} - \frac{1}{\tan(\theta + \frac{\sigma}{2})}, \tag{3}$$

where θ and σ are the elevation and size of the SG respectively. The resulting σ' corresponds to the size of the shadow penumbra (the softness of a shadow) produced by the light source. In this case, we assume a canonical unit height occluder casting a shadow on the floor perpendicular to the occluder (see supplementary details). The new σ' can be used in place of σ when constructing the 5D feature space.

4. Light feature vector

We denote the elevation, azimuth, and size of a given dominant light as θ, ϕ, and σ respectively. From Eq. (1), θ and ϕ are the angular components of **z**, while σ is the average of σ_x and σ_y. An RM may contain multiple dominant lights, thus an RM may contain multiple sets of these properties. To obtain a low-dimensional embedding, we describe a way of aggregating these dominant lighting properties into strictly three dominant light features: F_σ, F_θ, and F_c. The first two features describe the size and elevation, whereas the third takes into account the impact of multiple dominant lights, which describe as "complexity" or "angular spread". In addition to these dominant light features, we define the features F_s and F_h that describe the hue and saturation of the RM's diffuse shading. An overview of this process is shown in Fig. 2.

4.1. Dominant light features

After each dominant light Ω_j in an RM is fit by an instance of the DLM, the features of the RM are computed from the fitted DLMs. In the case that an RM contains more than one dominant light, there will be multiple DLMs producing $N \times 2$ light properties (σ, θ) for each of the N dominant lights. We identify the dominant light with the highest maximum intensity value as the *primary light*. The remaining $N-1$ dominant lights are *secondary lights*. The elevation and size features (F_θ, F_σ) are taken directly from the primary light's DLM θ and σ values. The primary light is chosen as it gives the user an intuitive handle on the most

visually striking effect the RM has on the rendered scene. We then aggregate the secondary light DLMs into a single feature F_c by considering the azimuthal relationship between the primary and secondary lights. To do this, we first define a weighted azimuthal distance as follows:

$$h(\phi_p, \phi_j) = \frac{|\phi_p - \phi_j|}{\pi} \cdot \log_{11}\left(\frac{a_j}{\sigma_j} \cdot \frac{1}{I} + 1\right), \tag{4}$$

which takes the normalized azimuth distance between the primary light's ϕ_p and the secondary light's ϕ_j and applies a logarithmic scaling factor. The scaling factor is a way of measuring how visibly apparent the light is by taking the light's mass $\frac{a_j}{\sigma_j}$ and dividing it by the total intensity of the RM I. Since this is a function of light intensity, we apply logarithmic scaling to be consistent with human perception. The overall effect of the scaling factor is to filter out secondary lights that are not as visually striking in their azimuthal spread of light/shadow. Finally, the feature is computed by taking the maximum value across all secondary dominant lights:

$$F_c = \max(h(\phi_p, \phi_j) : j = 1, \ldots, N). \tag{5}$$

A multiplicative sum across all secondary lights could be considered in order to ensure all dominant lights contributed to the feature. However, its physical meaning becomes less obvious. By using the max function, we can observe that a pair of dominant lights in an RM that were azimuthal opposite, with equal intensity, would become the highest possible azimuthal spread F_c. By introducing the RM's intensity I, the feature scales for each RM, giving those RMs with relatively brighter secondary lights a higher complexity value.

4.2. Ambient light features

The ambient illumination properties from an RM plays an important role in determining the mood and tone of a rendered image. We describe this effect with two features: the diffuse hue and saturation (F_h and F_s respectively). There are a number of possibilities for representing the overall color of an RM. It is intuitive if there is a 1-to -1 correspondence between the features and an exact matching color in the illuminated scene. For this reason, the features are set to the color of the diffusely filtered RM in the up direction. This corresponds to the color of a diffuse plane parallel with the floor.

In the browser application, the RM is given a preview of rendered objects on a diffuse floor. The floor provides a 1-to -1 correspondence with the color the users has selected to the returned results. Furthermore, artists often work with color temperatures, from cool to warm lighting. The features F_h and F_s is able to reproduce this effect with a distribution that spans across cool and warm tones, as shown Fig. 1 (left panel, bottom scatter plot).

5. Results

We evaluate the *illumination space* with various tasks including browsing, searching, and user interaction. We compare our method against recent work which also utilize RM databases.

5.1. Browsing the illumination space

We developed *'Illumination Browser'* to aid artists in exploring a parameterized RM database (Fig. 1). On the left panel, users are shown a visualization (two 2D scatterplots for dominant and ambient lighting) of the illumination space and are able to browse it by either using sliders or clicking inside the scatter plots. The results based on their input are in the center panel,
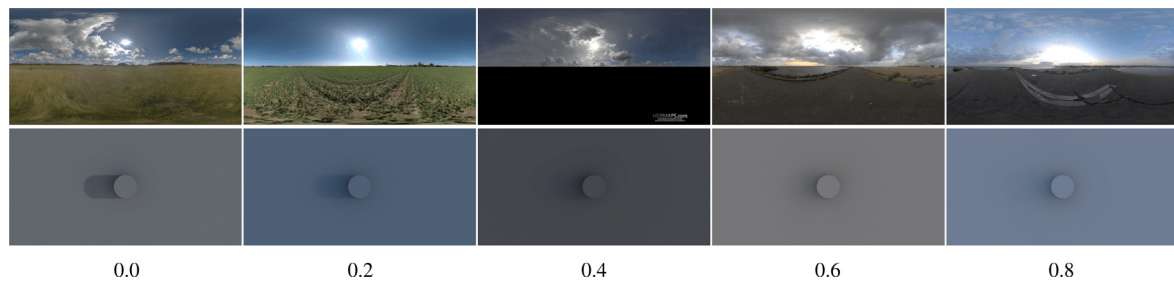
Fig. 3. Feature F_σ which shows the transition from hard to soft shadows. In the RM, this corresponds to the size of the dominant light source, transitioning from small to large. RMs with similar dominant light elevation F_θ are chosen.
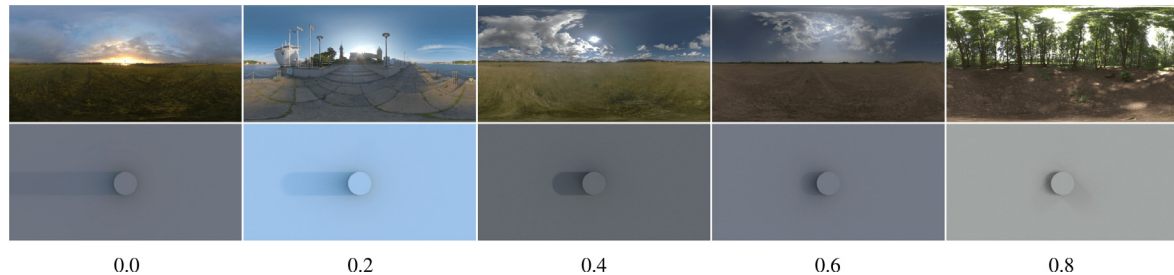

Fig. 4. Feature F_θ which shows the transition from long to short shadows. In the RM, this corresponds to the elevation of the dominant light source, transitioning from low to high. RMs with similar shadow softness F_σ are chosen.
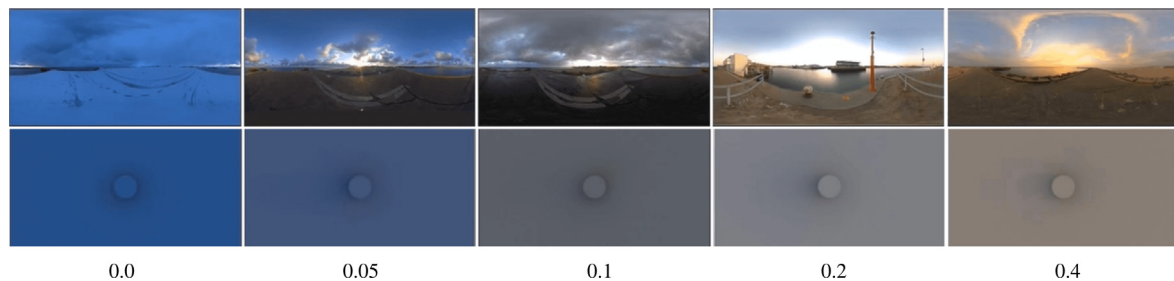

Fig. 5. Feature F_h and F_s are the color features. It is common to find RMs with either red (indoor, sunset), blue (clear sunny sky) or desaturated colors (indoor, overcast). This corresponds to a cool/warm color distribution. We visualize the transition from high saturation blue, desaturated, and high saturation red in one dimension (left to right).
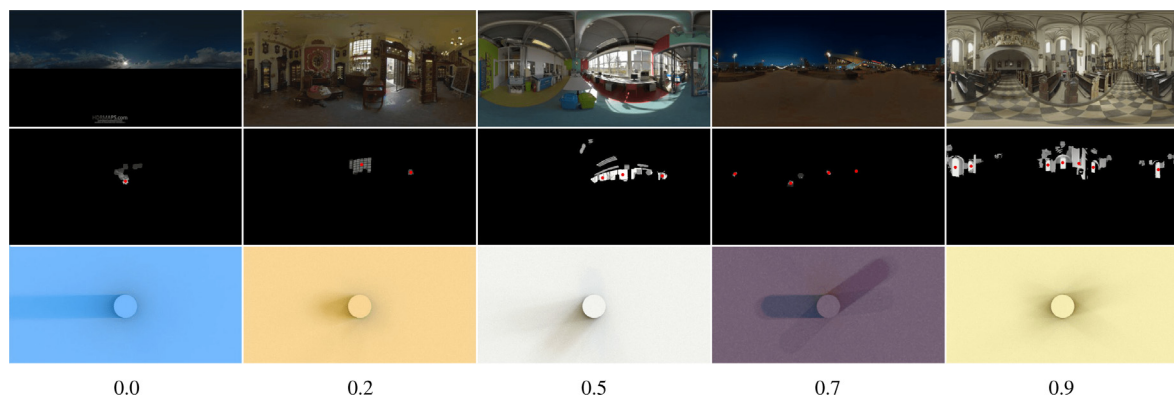

Fig. 6. Feature F_c which shows the transition from low to high azimuthal spread. The center row shows how it corresponds to the number of detected dominant lights (red dots have been added to the center of each detected dominant light source). The rendered images have been normalized to show the details.

which shows the RMs in the database which are closest to the user input. Each returned RM is also shown with a corresponding shadow-profile image to illustrate its illumination properties. Browsing the database runs at interactive rates using optimized
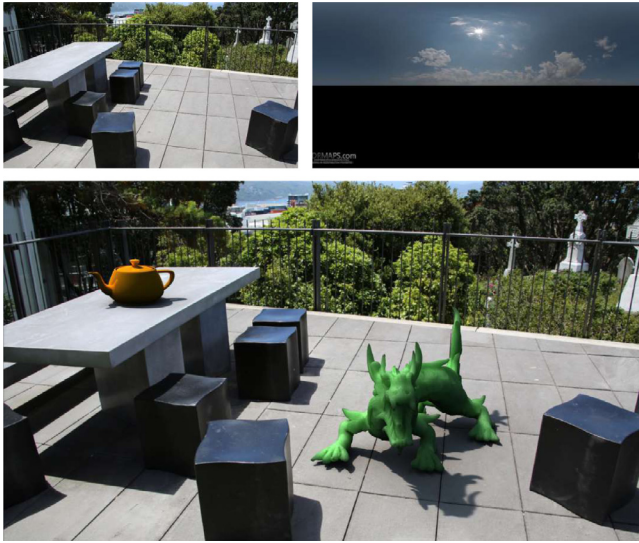
Fig. 7. The light features are obtained from the shadow profile from the photograph (top left) and are used to look up an RM from the database with similar illumination (top right). The green dragon and orange teapot are composited into the photograph (bottom).

KNN algorithms [57]. The artist is able to select an RM from the center-panel to then illuminate three spheres with a mirror, glossy, and diffuse material on a diffuse, shadow-catching plane, shown in the right-panel. The right panel is a custom interactive real-time ray tracer to render the mirror/glossy/diffuse spheres (using the GGX [58] and Lambertian model). The user is able to click inside the rendering window to rotate the camera. Note that because the dimensions are split across two 2D scatter plots (left panel), it can be difficult to identify where a point in one plot corresponds to in the other plot. To alleviate this, the transparency channel of the dominant light points are weighted by the distance between the user input and the point's corresponding position in the ambient scatter plot, and vice versa for setting the transparency for the ambient light points. The complexity is shown by coloring the dominant light points along a color spectrum, along with coloring the complexity slider's background color as well. The result is that the user is able to clearly see where clusters exists based on their input. See the supplementary video for this interaction.

Figs. 3, 4, and 6 show examples of gradually browsing along light size (shadow softness), elevation (shadow length), and the azimuthal spread with features F_σ, F_θ, and F_c respectively. In each case, some features are constrained while others are not. For example, Fig. 3 demonstrates modifying F_σ while F_θ is constrained. This maintains the shadow length (light elevation) while F_σ adjusts the shadow softness (light size). Other parameters such as the tone features F_h and F_s are varying. We observe that the RMs often appear in one of two color distributions (the peaks of hue in Fig. 1). We visualize the cool to warm transition in one dimension in Fig. 5.

5.2. Searching the illumination space

We show an example usage of a search query by manually-identifying a shadow profile and its corresponding object to then infer the light feature vector (Fig. 7). Search-based tasks can also use an RM as input to query the RM database in order to find similar illumination. To do this, we simply project the new RM into the database using the same feature extraction methods. As such, an example RM provided from artists (e.g., captured on set,

or a light estimated RM in AR applications) can be used to find other similar illumination (Fig. 8 shows some examples of using an RM to query the database for another similar RM).

5.3. User evaluation and comparison

We had nine artists use 'Illumination Browser' to search for RMs. They were told to first familiarize themselves with its features. Following this, they were tasked to illuminate a synthetic object (which is composited into a photograph) with an RM obtained from the database (no time limit was given, but on average users took approximately 2 min per task). The artists did this for nine different photographs, covering a wide range of illumination conditions (see the supplementary materials on selected photographs and example compositions). After this, the artists were asked to qualitatively evaluate each feature individually on how well it met their expectations on a 5-point Likert item (from −2, to 2). We found that the features visualized directly on the scatter plots (elevation, size, hue, and saturation) were very intuitive with a median score of 2 with little deviation. Users commented that the azimuthal spread was useful but not as intuitive due to few samples being returned during the browsing and difficulty seeing the clustering in the third dimension (median score of 1).

Following this, we took three example RMs of varying properties (in both high and low frequency details, see Fig. 8), and queried the database to find the most similar RM to each of the three examples, comparing our method with [29]. We asked users to choose which method obtained the most similar result (based on the illuminated scene) compared with the input RM's illuminated scene. Participants preferred our results 85.2% of the time. To demonstrate the utility of the illumination space for rendering tasks, Fig. 9 shows examples of compositing synthetic objects into photographs using RMs selected using 'Illumination Browser'.

6. Conclusion and future work

This paper presents a set of light features that describe the illumination properties of an RM. The features themselves are concise and intuitive, presented as a 5D feature vector, describing both high and low frequency details. The features have a direct correspondence between the light source and its impact on the rendered scene. By introducing a dominant light model, fitting algorithm, and lights features, it is possible to automatically parameterize a large database of RMs into low dimensional features. Furthermore, ambient light features describing color and tone allows for a complete feature descriptor of RMs, describing both high and low frequency details. From these features, we are able to construct a lighting-based feature space – the 'illumination space' – that arranges RM databases. We also introduce 'Illumination Browser', a user interface that brings out the full potential of the illumination space for browsing and searching applications.

Future work can consider methods of overcoming sparsity in RM databases, which can make it difficult to browse if few samples exist. We also found that the vast majority of our database contained near-white high frequency lighting, so we neglected to give artists the ability to specify high frequency colors. In our work, we do not directly encode anisotropic lighting, multiple shadows, high frequency color, or contrast. Future work can attempt to include parameters to encompass these effects (e.g., via MDS or t-SNE) while still being able to obtain sensible results from the RM database in an artist friendly way. Integrating our browser with prior related systems [6,23,59] could be considered to fully utilize RM databases across lighting, texture and artist modification.
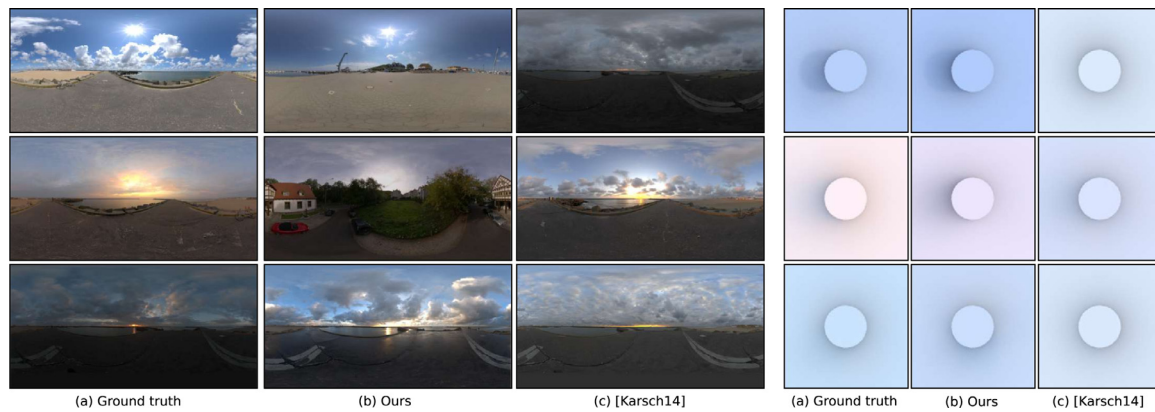
Fig. 8. Querying the database with the input (ground truth), we compare our result with [Karsch14]. Our method maintains similarities with the ground truth in both light (RM, left) and illumination properties (rendered scene, right).

Fig. 9. Examples of compositing into a photograph, where the RM was selected by a user using 'Illumination Browser'. Inserted objects are: (left) Stanford Dragon and Bunny, (center) Stanford Asian Dragon, and (right) cylinder.

CRediT authorship contribution statement

Andrew Chalmers: The researcher who carried out the experiments, Implementation. **Todd Zickler:** Supervisors who provided guidance, Direction on the research. **Taehyun Rhee:** Supervisors who provided guidance, Direction on the research.

Declaration of competing interest

One or more of the authors of this paper have disclosed potential or pertinent conflicts of interest, which may include receipt of payment, either direct or indirect, institutional support, or association with an entity in the biomedical field which may be perceived to have potential conflict of interest with this work. For full disclosure statements refer to https://doi.org/10.1016/j.cag.2022.01.006.

Victoria University of Wellington (institute), Harvard University (institute), Ministry of Business and Educaton (funding), Tertary Educaton Commission (funding).

Funding

Appendix A. Supplementary data

Supplementary material related to this article can be found online at https://doi.org/10.1016/j.cag.2022.01.006.

References

[1] Gardner M, Sunkavalli K, Yumer E, Shen X, Gambaretto E, Gagné C, et al. Learning to predict indoor illumination from a single image. ACM Trans Graph (SIGGRAPH Asia) 2017.

[2] Hold-Geoffroy Y, Sunkavalli K, Hadap S, Gambaretto E, Lalonde J-F. Deep outdoor illumination estimation. In: IEEE international conference on computer vision and pattern recognition. 2017.

[3] Chalmers A, Zhao J, Medeiros D, Rhee T. Reconstructing reflection maps using a stacked-CNN for mixed reality rendering. IEEE Trans Vis Comput Graph 2020;1. http://dx.doi.org/10.1109/TVCG.2020.3001917.

[4] Hosek L, Wilkie A. An analytic model for full spectral sky-dome radiance. ACM Trans Graph 2012.

[5] Ramamoorthi R, Hanrahan P. An efficient representation for irradiance environment maps. SIGGRAPH '01, ACM; 2001.

[6] Chalmers A, Zickler T, Rhee T. Illumination space: A feature space for radiance maps. The Eurographics Association; 2020.

[7] Tsai Y-T, Shih Z-C. All-frequency precomputed radiance transfer using spherical radial basis functions and clustered tensor approximation. Trans Graph 2006.

[8] Xu K, Sun W-L, Dong Z, Zhao D-Y, Wu R-D, Hu S-M. Anisotropic spherical Gaussians. ACM Trans Graph 2013;32(6):209:1–209:11.

[9] Cox MA, Cox TF. Multidimensional scaling. In: Handbook of data visualization. Springer; 2008, p. 315–47.

[10] Yang J, Fan J, Hubball D, Gao Y, Luo H, Ribarsky W, et al. Semantic image browser: Bridging information visualization with automated intelligent image analysis. In: 2006 IEEE symposium on visual analytics science and technology. IEEE; 2006, p. 191–8.

[11] Mizuno K, Wu HY, Takahashi S. Manipulating bilevel feature space for category-aware image exploration. In: 2014 IEEE pacific visualization symposium. IEEE; 2014, p. 217–24.

[12] Schubert E, Gertz M. Intrinsic t-stochastic neighbor embedding for visualization and outlier detection. In: International conference on similarity search and applications. Springer; 2017, p. 188–203.

[13] Luo X, Scandolo L, Eisemann E. Texture browser: Feature-based texture exploration. In: Comput Graph Forum. 2021;40(3):99–109.

[14] Johnson M, Brostow GJ, Shotton J, Arandjelovic O, Kwatra V, Cipolla R. Semantic photo synthesis. Comput Graph Forum 2006;25(2):407–12.

[15] Lalonde J-F, Hoiem D, Efros AA, Rother C, Winn J, Criminisi A. Photo clip art. ACM Trans Graph 2007;26(3).

[16] Laffont P-Y, Ren Z, Tao X, Qian C, Hays J. Transient attributes for high-level understanding and editing of outdoor scenes. ACM Trans Graph (Proceedings of SIGGRAPH 2014) 2014;33(4).

[17] Oliva A, Torralba A. Modeling the shape of the scene: A holistic representation of the spatial envelope. Int J Comput Vis 2001.

[18] Hoiem D, Efros AA, Hebert M. Geometric context from a single image. In: Tenth IEEE international conference on computer vision, 2005, vol. 1. IEEE; 2005, p. 654–61.

[19] Lazebnik S, Schmid C, Ponce J. Beyond bags of features: Spatial pyramid matching for recognizing natural scene categories. In: 2006 IEEE computer society conference on computer vision and pattern recognition, vol. 2. IEEE; 2006, p. 2169–78.

[20] Tao L, Yuan L, Sun J. Skyfinder: Attribute-based sky image search. In: Proc. of ACM SIGGRAPH 2009. ACM; 2009, p. 68:1–5.

[21] Ono A, Dobashi Y, Yamamoto T. A system for editing sky images using an image database. In: SIGGRAPH Asia 2011 Sketches. SA '11, ACM; 2011, p. 38:1–2.

[22] Mitani T, Fujishiro I. CosmicAI: Generating sky backgrounds through content-based search and flexible composition. In: ACM SIGGRAPH 2012 Posters. ACM; 2012, p. 51–2.

[23] Chalmers A, Lewis J, Hillman P, Tait C, Rhee T. Sky browser: Search for HDR sky maps. In: Pacific Graphics. The Eurographics Association; 2014.

[24] Pellacini F, Ferwerda JA, Greenberg DP. Toward a psychophysically-based light reflection model for image synthesis. In: Proc. of SIGGRAPH '00. 2000.

[25] Wills J, Agarwal S, Kriegman D, Belongie S. Toward a perceptual space for gloss. ACM Trans Graph 2009;28(4):103:1–103:15.

[26] Serrano A, Gutierrez D, Myszkowski K, Seidel H-P, Masia B. An intuitive control space for material appearance. ACM Trans Graph 2016.

[27] Gkioulekas I, Xiao B, Zhao S, Adelson EH, Zickler T, Bala K. Understanding the role of phase function in translucent appearance. ACM Trans Graph 2013;32(5):147:1–147:19.

[28] Papas M, Regg C, Jarosz W, Bickel B, Jackson P, Matusik W, et al. Fabricating translucent materials using continuous pigment mixtures. ACM Trans Graph 2013.

[29] Karsch K, Sunkavalli K, Hadap S, Carr N, Jin H, Fonte R, et al. Automatic scene inference for 3D object compositing. ACM Trans Graph 2014.

[30] Bloch C, Bauer C, Heisterberge V, Reddick G, chris H. Smart-IBL. SIGGRAPH Course Notes, 2008, http://www.hdrlabs.com/sibl/. [Accessed 30 June 2020].

[31] Lalonde J-F, Efros A, Narasimhan S. Estimating the natural illumination conditions from a single outdoor image.. Int J Comput Vis 2012.

[32] Xing G, Zhou X, Peng Q, Liu Y, Qin X. Lighting simulation of augmented outdoor scene based on a legacy photograph. Comput Graph Forum 2013;32(7):101–10.

[33] Gardner M-A, Hold-Geoffroy Y, Sunkavalli K, Gagne C, Lalonde J-F. Deep parametric indoor lighting estimation. In: The IEEE international conference on computer vision. 2019.

[34] Garon M, Sunkavalli K, Hadap S, Carr N, Lalonde J-F. Fast spatially-varying indoor lighting estimation. In: Proceedings of the IEEE conference on computer vision and pattern recognition. 2019, p. 6908–17.

[35] LeGendre C, Ma W-C, Fyffe G, Flynn J, Charbonnel L, Busch J, et al. Deeplight: Learning illumination for unconstrained mobile mixed reality. In: Proceedings of the IEEE conference on computer vision and pattern recognition. 2019, p. 5918–28.

[36] Song S, Funkhouser T. Neural illumination: Lighting prediction for indoor environments. In: Proceedings of the IEEE conference on computer vision and pattern recognition. 2019, p. 6918–26.

[37] Chalmers A, Zhao J, Medeiros D, Rhee T. Reconstructing reflection maps using a stacked-CNN for mixed reality rendering. IEEE Trans Vis Comput Graph 2020.

[38] Zhao J, Chalmers A, Rhee T. Adaptive light estimation using dynamic filtering for diverse lighting conditions. IEEE Trans Vis Comput Graph 2021;27(11):4097–106.

[39] Einabadi F, Guillemaut J-Y, Hilton A. Deep neural models for illumination estimation and relighting: A survey. Comput Graph Forum 2021.

[40] Sloan P-P, Kautz J, Snyder J. Precomputed radiance transfer for real-time rendering in dynamic, low-frequency lighting environments. SIGGRAPH 2002, ACM; 2002.

[41] Ng R, Ramamoorthi R, Hanrahan P. All-frequency shadows using non-linear wavelet lighting approximation. In: Proc. of ACM SIGGRAPH 2003. ACM; 2003.

[42] Debevec P. A median cut algorithm for light probe sampling. In: ACM SIGGRAPH 2006 Courses. ACM; 2006.

[43] Viriyothai K, Debevec P. Variance minimization light probe sampling. In: SIGGRAPH'09: Posters. ACM; 2009, p. 92.

[44] Agarwal S, Ramamoorthi R, Belongie S, Jensen HW. Structured importance sampling of environment maps. ACM Transa Graph 2003.

[45] Lu H, Pacanowski R, Granier X. Real-time importance sampling of dynamic environment maps. In: EG 2013 - Short papers. 2013.

[46] Hold-Geoffroy Y, Athawale A, Lalonde J-F. Deep sky modeling for single image outdoor lighting estimation. In: Proceedings of the IEEE/CVF conference on computer vision and pattern recognition. 2019, p. 6927–35.

[47] Cheng D, Shi J, Chen Y, Deng X, Zhang X. Learning scene illumination by pairwise photos from rear and front mobile cameras. Comput Graph Forum 2018;37(7):213–21.

[48] HDRIHaven. HDRIHaven [Radiance maps database]. 2020, https://hdrihaven.com/hdris/. [Accessed 30 June 2020].

[49] OpenFootage. OpenFootage [RAdiance maps database]. 2017, http://www.openfootage.net/. [Accessed 30 June 2020].

[50] HDRIHub. HDRI Hub [Radiance maps database]. 2017, http://www.hdri-hub.com/. [Accessed 30 June 2020].

[51] DutchSkies360. Dutch skies 360 [Radiance maps database]. 2017, http://www.dutch360hdr.com/. [Accessed 30 June 2020].

[52] HDRSource. HDR Source [Radiance maps database]. 2017, http://www.hdrsource.com/. [Accessed 30 June 2020].

[53] HDRLabs. HDR Labs [Radiance maps database]. 2017, http://www.hdrlabs.com/sibl/archive.html. [Accessed 30 June 2020].

[54] HDRMaps. HDR Maps [Radiance maps database]. 2017, http://hdrmaps.com/. [Accessed 30 June 2020].

[55] Rhee T, Petikam L, Allen B, Chalmers A. Mr360: Mixed reality rendering for 360 panoramic videos. IEEE Trans Vis Comput Graph 2017;(4):1379–88.

[56] Voglis C, Lagaris I. A Rectangular Trust Region dogleg approach for unconstrained and bound constrained nonlinear optimization. In: WSEAS Conference. 2004, p. 17–9.

[57] Muja M, Lowe DG. Scalable nearest neighbor algorithms for high dimensional data. IEEE Trans Pattern Anal Mach Intel 2014;36.

[58] Walter B, Marschner SR, Li H, Torrance KE. Microfacet models for refraction through rough surfaces. Render Tech 2007;2007:18th.

[59] Pellacini F. Envylight: An interface for editing natural illumination. In: ACM SIGGRAPH 2010 papers. 2010, p. 1–8.